Thermodynamic and Kinetics Aspects of High Temperature Oxidation on a 304L Stainless Steel

Thermodynamic and kinetics aspects of high temperature oxidation on a 304L stainless steel

D. Lussana[1], D. Baldissin[1,2], M. Massazza[3], M. Baricco[1]

[1] Università di Torino, Dipartimento di Chimica and NIS, Torino, Italy

[2] Compumat Srl, Torino, Italy

[3] Cogne Acciai Speciali Spa, Aosta, Italy

Introduction

Several steps at high temperature are involved during the production process of stainless steels. They lead to the formation of an oxide layer at the surface, and its removal strongly influence the quality of the final product and the production costs.

Several models for the oxide growth on stainless steels are present in the literature [1-5]. They can be summarized considering the formation of a chromia (Cr_2O_3) layer at low temperatures, which acts as a protective barrier against further oxidation. At higher temperatures, the chromia layer starts to transform into a spinel type oxide M_3O_4 (M = [Cr, Fe]). During growth, it becomes progressively richer in iron, up to the transformation in hematite (Fe_2O_3). The growth of the oxide layer can be described according to the Wagner model [6]. It considers a parabolic law in order to describe the weight increase as a function of the time. Every single oxide is characterized by its own parabolic rate constant, k_p.

The limitations of these models in describing the high temperature oxidation of stainless steel are evident. It must be noted that oxidation is a continuous transformation, with a virtually infinite availability of reagents. It proceeds on two interfaces, the oxide/gas and the oxide/metal, at which

very different oxygen partial pressure are present and, hence, different reactions could take place. Moreover, the developed oxides are very defective, often with non stoichiometric composition. Finally, the breakaway oxidation phenomenon [7] can randomly superimpose on the oxidation, drastically changing its time evolution. Most of experimental data available in the literature have been collected for tens of hours of oxidation, without providing reliable models for the first few hours, which are, however, those involved in the industrial production process.

Aim of this study is the setting up of a simple model able to describe the main feature of the high temperature oxidation on the surface of an AISI 304L stainless steel in industrial-like conditions. A combination of optimised thermodynamic phase diagrams and experimental kinetic data will be provided to describe oxidation processes.

Experimental

Wired rods (21 mm diameter) of commercial AISI 304L steel (nominal composition in Table 1) were provided by Cogne Acciai Speciali.

Table 1 – Composition of AISI 304L stainless steel, wt%

Samples were cut from the core of the rods and prepared in the form of parallelepiped of about 3x3x1 mm^3. All the surfaces were finished with a 1200 emery paper.

The samples were oxidised in a TA 600 DTA/TGA instrument, which recorded the weight increase during isothermal annealing. The oxidising atmosphere was prepared starting from synthetic air and pure nitrogen, mixed by means of a mass flow controller. The selected oxygen partial pressure was 0.087 atm, similar to that found in an industrial furnace for stainless steel heat treatment. The measurement proceed in three steps: in the first, the samples were heated up at 20 K min^{-1} to the target

temperature in pure nitrogen, in order to avoid oxidation during the heating. Then, they were kept at the set up temperature for 10 minutes in order to equilibrate the system. Finally, the nitrogen is substituted with the oxidising gases, and data are collected.

X-ray diffraction analyses (XRD) of the annealed samples were performed with a Panalyitical X'pert diffractometer with a Cu radiation and a Bragg-Brentano geometry. In order to obtain the phase fraction on each sample, a Rietveld refinement [8] of XRD patterns was performed with the MAUD software [9].

The phases present in the equilibrium conditions and their fractions as a function of temperature and of oxygen partial pressure were calculated using the Calphad approach (Thermocalc software). The thermodynamic database was built on the basis of recent literature [10-13].

Results and discussion

Characterization of the oxide layer

Figure 1a shows the TGA curves obtained annealing the AISI 304L stainless steel for three hours in 0.087 atm of oxygen partial pressure in the range of temperatures from 800 °C to 1200 °C. For comparison, the TGA curve of a sample annealed three hours at 1050 °C in a pure nitrogen atmosphere is also reported, showing an almost null weight increase. As expected from simple kinetic considerations, the higher the temperature of annealing, the grater the weight gain after the same annealing time. It is worth noting the good reproducibility of measurements, as shown by the two curves obtained at 1050 °C with two different samples in the same conditions.

Figure 1 – a) TGA curves (symbols, only selected points are reported) and curves fitted according to eq. 3 (continuous lines) of samples annealed 3 hours in 0.087 atm of oxygen partial pressure at the indicated temperatures. Small empty circles represent the TGA curve of a sample annealed 3 hours at 1050 °C in a pure nitrogen atmosphere. b)

Comparison among the TGA curve at 800 °C (squares), the fitted curve according to eq. 3 (continuous line) and the fitted curve according to eq. 1 (dashed line)

In order to identify the oxides formed during the annealing, XRD analyses were performed after the annealing treatments (figure 2). Reflections of the bulk phases (austenite and ferrite) are present in all samples. The presence of a ferrite phase is somehow unexpected in an austenitic steel, even if it has been already reported in the literature [3] for samples similarly treated. It can be connected to the local change of composition of the steel just below the oxide layer. The intensities of the bulk phases reflections are very high in comparison with those of the oxides reflections, making difficult the identification of the latter. It is however possible to distinguish the reflections of chromia (Cr_2O_3) and hematite (Fe_2O_3), which have a similar corundum structure, together with the reflections of the mixed phase M_3O_4 (M=[Fe,Cr]), with a spinel structure. Among the oxides, only reflections of the chromia phase are clearly observed at 800 °C. The signals of the spinel phase progressively increase up to 1000 °C. Finally, reflections of the hematite phase are prevalent at higher temperatures.

In order to perform quantitative analysis of phase fraction, a XRD measurement with higher acquisition time, and hence with a higher signal-to-noise ratio, was performed for a samples annealed in industrial-like conditions (that is 2 hours at 1050 °C and 0.087 atm of oxygen partial pressure). The Rietveld analysis of this pattern was carried out considering the bulk phases (austenite fcc and ferrite bcc) and the Cr_2O_3, Fe_2O_3 and M_3O_4 oxide phases. For the spinel type phase, it was impossible to separate the contribution of magnetite Fe_3O_4 and chromite $FeCr_2O_4$ because they form a continuous solid solution with a transition from a direct to an inverse spinel [14]. So, a mixed phase $Fe^{2+}Cr^{3+}_{2x}Fe^{3+}_{2-2x}O_4$ was built from $FeCr_2O_4$, imposing a vicariancy between Cr^{3+} and Fe^{3+}. The results of the Rietveld refinement of the XRD pattern, corresponding goodness-of-fit R_w=1.3, is reported in figure 3, giving the following phase fraction (weight percent): 20% of Cr_2O_3 and 51% of Fe_2O_3 (total 71% corundum phase), and 29% of spinel phase. Because of

the layered nature of samples, accurate corrections for penetration depth and absorption should be considered in Rietveld refinement. In the present experimental conditions, the contribution of the bulk metallic phases present under the oxide layer to the XRD spectra are rather significant, making corrections negligible. In fact, an XRD analyses performed on oxide powders obtained from a chemical etching of the oxidized sample provided very similar results.

Figure 2- XRD patterns of AISI 304L samples annealed 2 hours at different temperatures in 0.087 atm of oxygen partial pressure. The inset on the top shows the calculated positions and relative intensities of diffraction peaks for the reported phases. The square root of intensity is reported.

Figure 3 - Experimental data (empty circles) and Rietveld refined intensity (continuous line) of an AISI 304L sample annealed 2 hours at 1050 °C in 0.087 atm of oxygen partial pressure, together with residuals. The square root of intensity is reported.

Thermodynamic analysis

In order to compare the experimental data with the equilibrium conditions, a phase diagrams has been calculated by the Calphad approach, using the Thermocalc software. Figure 4a shows the stable phases present in the AISI 304L steel under oxidising atmosphere as a function of temperature and oxygen partial pressure; figure 4b shows the mutual quantities of the phases as a function of the temperature, and figure 4b shows the mutual quantities of the phases as a function of the oxygen partial pressure.

Figure 4 – a) Calculated phase diagram of the AISI 304L – oxygen system; b) relative quantities of spinel and corundum oxide phase at 0.087 atm oxygen partial pressure as a function of the temperature; c) relative quantities of spinel and corundum oxide phase at 1050 °C as a function of the oxygen partial pressure. Dashed lines indicate the industrial-like conditions (0.087 atm of oxygen partial pressure and 1050 °C). Gas fraction in figures b) and c) is below 0.01

The calculations in equilibrium for the industrial-like conditions (i.e. 0.087 atm of oxygen partial pressure and 1050 °C) give the presence of 55% of corundum phase with an average composition $Fe_{1.4}Cr_{0.6}O_3$, and 45% of spinel phase with an average composition $Fe_{1.3}Cr_{0.9}Ni_{0.8}O_4$. The comparison of calculation results with experimental data indicates a kinetic reaction control for samples treated for 2 hours at 1050 °C in the TGA instrument, as confirmed by the absence of a clear steady state at the end of the measurements. Hence, the role of the kinetic parameters must be taken into account in order to describe the observed oxide layers.

Kinetic analysis

A logarithmic growth law for oxidation of iron and steel is usually acting a low temperatures (i.e. < 300 °C) [15, 16]. At higher temperatures (i.e. > 800 °C), the growth kinetics of an oxide layer on steel is often described according to Wagner model [6]. Accordingly, the weight increase as a function of time follows a parabolic law, and thus the oxidation can be described with:

$$W(t) = k\sqrt{t} \qquad \text{eq. 1}$$

where $W(t)$ is the weight gain of the oxide at the time t of the annealing, and k is the rate constant. After fitting of experimental data reported in figure 1, the rate constants have been calculated according to eq. 1 and they are reported in table 2. However, in the present cases, a transient stage before the parabolic behaviour is clearly present. This stage is more evident for the TGA curves obtained at the lowest temperatures, as shown in figure 1b for an annealing at 800 °C.

The lack of a single rate constant during oxidation of AISI 304L has been already observed [1,17] and two separate parabolic rate constant have been considered. They have been associated to the formation of chromia and haematite or magnetite oxide phases, separated by a transient stage where a codevelopment of different oxide phases is occurring. On the other hand, it is known from the literature [15] that a simple parabolic law is often not sufficient to describe accurately the kinetics of oxidations. In these cases, the mixed parabolic model is often considered, so that an initial linear growth behaviour is taken into account. This model has been widely applied for describing

oxidation in Cu [18] and Si [19]. It has been also considered for steels with various composition [20], considering that at the start of oxidation, the rate of reaction is driven by the supply of the oxidising gas to the reaction zone, so that a linear behaviour is observed. In addition, a similar behaviour is expected if the scale produced is porous, so that it does not act as a barrier to further oxidation. On the contrary, if a compacted scale is formed for longer annealing times, the rate of scale growth is controlled by diffusion of reaction species through developing oxide layer. As a consequence, a parabolic growth rate is expected [15]. Formation of cracks within the scale can act as short-cuts for the gas phase or barriers for ionic diffusion.

For these reasons, a linear term in addition to the parabolic one is introduced in the eq. 1 in the form of

$$W(t) = k_l t + w_0 \qquad \text{eq. 2}$$

where k_l is the linear rate constant. w_0 is imposed equal to 0, i.e. at the beginning of the annealing the weight of the very thin chromia layer, always present on the surface of a AISI 304L steel stored in an air atmosphere, is negligible.

The two terms (linear and parabolic) are weighted with a function $\chi(t) = e^{\frac{-t^2}{\sigma}}$, so that the contribution of the linear term is maximum when t tends to zero ($\chi(0)=1$), and minimum when t tends to infinite ($\chi(\infty)=0$) and σ is a parameter which describe the sharpness of the transition between linear and parabolic growth behaviour.

Hence, the weight increase as a function of time can be described according to:

$$W(t) = e^{\frac{-t^2}{\sigma}} k_l t + (1 - e^{\frac{-t^2}{\sigma}}) k_p \sqrt{t} \qquad \text{eq. 3}$$

where k_p is the parabolic rate constant.

The experimental TGA curves have been fitted with eq. 3, and the results are reported in figure 1 (continuous lines). The fit is good, in particular at the beginning of oxidation, where a simple parabolic trend failed to reproduce the experimental curves (figure 1b). In this way, it is possible to

obtain the linear constant (k_l) and a more accurate parabolic constant (k_p) for each curve. The corresponding values are reported in table 2, together with the sharpness parameter (σ).

Table 2 –Rate constant (k) according to eq. 1, and σ parameter, linear constant (k_l) and parabolic constant (k_p) according to eq. 3, obtained from fit of the TGA curves of figure 1

Obtained results are in good agreement with parabolic rate constant obtained for an AISI 304L steel in the same temperature range and in similar oxidation atmosphere [1]. The values of k_p and k_l increase as a function of temperature, as expected. It is worth noting that increasing the temperature of annealing, the value of σ moves toward lower values, corresponding to a faster transition from the linear trend to the parabolic one. This is in agreement with the hypothesis that the higher the temperature, the faster the oxidation, and thus the lower the time needed to reach the parabolic trend.

Figure 5 – Arrhenius plots of rate constants according to eq. 1 (x-symbols), linear constants (triangles) and parabolic constants according to eq.3 (squares) and corresponding liner fit (dotted and dashed lines, respectively).

The evolutions of the k_l and k_p as a function of temperature are reported as an Arrhenius plot (figure 5), together with the values of k. Hence, from the slope of the linear fit of the natural logarithm of k_l [21] and of k_p^2 (or k^2) [6] as function of $1/T$, it is possible to calculate the value of the apparent activation energies for the oxidation. In the present case, using eq. 1, the obtained value is 117 kJ mol^{-1}. Using eq. 3, the apparent activation energies are 96 ± 19 kJ mol^{-1} for the linear part of the oxidation, and 138 ± 12 kJ mol^{-1} for the parabolic one. The activation energy for oxidation in AISI 304L seems to be strongly influenced by the atmosphere, ranging from 150 up to 323 kJ mol^{-1} [1]. Obtained data represent only an apparent value for the activation energy for reactions which take

place simultaneously during the first three hour of oxidation. Nonetheless, considering the good reproducibility of the experimental TGA curves, they can be taken as characteristic values for the oxidation of the AISI 304L stainless steel under the present conditions.

Growth model

The values of the parabolic constant for the growth of single oxides can be calculated from the equation obtained by Hindam and Whittle [1,22]:

$$k_s = \frac{1}{RT}\int_{p_{in}O_2}^{p_{ex}O_2}\left(D_a + \frac{|z_c|}{z_a}D_c\right)d\ln p(O_2) \qquad \text{eq. 4}$$

where k_s is the parabolic constant when the increase of the thickness (instead of weight) of the oxide layer is considered; $p_{ex}(O_2)$ and $p_{in}(O_2)$ are the oxygen partial pressure at the gas-oxide and oxide-metal interfaces, respectively; z_c and z_a are the valences of the cation and anion, respectively; D_c and D_a are the diffusion coefficients for the cation and anion, respectively. Considering the concentration of defects in the oxide independent from the oxygen partial pressure, it follows [22]:

$$k_s = \frac{1}{RT}\left(D_a + \frac{|z_c|}{z_a}D_c\right)\int_{p_{in}O_2}^{p_{ex}O_2} d\ln p(O_2) = \frac{1}{RT}\left(\frac{z_c}{z_a}D_c + D_a\right)\ln\frac{p_{ex}(o_2)}{p_{in}(o_2)} \qquad \text{eq. 5}$$

The weight increase, w, and the thickness, x, of the oxide layer are linked each other with the following relation [23]:

$$w = \frac{nM_o}{M_{ox}}\rho_{ox}x \qquad \text{eq. 6}$$

where, M_o an M_{ox} are the molecular mass of the oxygen and of the oxide respectively, n is the number of oxide atoms per formula unit of oxide, and ρ_{ox} is the density of the oxide. From eq. 6 it follows:

$$k_c = \left(\frac{nM_o}{M_{ox}}\right)^2 k_s \qquad \text{eq. 7}$$

Using the values of the oxygen partial pressure from the work of Huntz et al. [1], and the diffusion coefficients from the work of Tsai et al. [23], it is possible to calculate the values of k_s for Cr_2O_3,

Fe_2O_3 and M_3O_4 at 1050 °C. Finally, using eq. 7, it is possible to calculate the value of the parabolic rate constants, k_c, for each oxide phase.

Table 3 shows the values of k_p of the sample treated in industrial-like conditions and k_c for the single oxides, calculated according to eq. 7. The experimental results of k_p falls inside k_c calculated values of the hematite, spinel, and chromia, confirming that all different oxides contribute to the oxidation. However, according to the general models of the oxidation [1-5], the contributions of the single oxides are not constant during the annealing, and thus it is not possible to separate them only from the values of the parabolic constants.

Table 3 – Comparison between experimental (k_p^2)and calculated (k_c^2) parabolic rate constants at 1050 °C. The experimental value is the average of the values calculated from the two TGA curves at 1050 °C and 0.087 atm of oxygen partial pressure. Data in $g^2\ cm^{-4}\ s^{-1}$.

For this purpose, it was necessary to collect quantitative data on the oxides present in the oxide layer after different time of annealing. Hence, XRD measurements were performed on samples annealed in the TGA instruments at 1050 °C and 0.087 atm of oxygen partial pressure for different times up to three hours (figure 6), and then the fractions of all oxides were obtained by means of Rietveld analysis. The weight fractions of the oxide phases are reported in figure 7 as a function of annealing time. The values at t=0 were chosen considering that, prior to any annealing, only a thin protective chromia layer is present on an AISI 304L steel stored in an air atmosphere. A $Fe^{2+}Cr^{3+}_{2x}Fe^{3+}_{2-2x}$ phase was used for the spinel type oxide, and the corresponding x values are also reported in figure 7. As expected, the value of x indicates a progressive enrichment of Fe in the spinel type oxide as the annealing treatment proceeds.

Figure 6 – XRD patterns of samples treated at 1050 °C and 0.087 atm of oxygen partial pressure for the indicated times. The inset on the top shows the calculated positions and relative intensities of diffraction peaks for the reported phases. The square root of intensity is reported.

Figure 7 –Experimental (points) and calculated (lines) weight fraction of Cr_2O_3, M_3O_4 and Fe_2O_3 in the oxide layer as a function of the annealing time at 1050 °C and 0.087 atm of oxygen partial pressure. Values of the parameter x(x-symbols) calculated from Rietveld analysis are also reported.

The complete description of the oxidation involves several reactions which take place simultaneously during heating. However, it can be sketched with a simple model of two successive first order reaction: the first one accounts for all the reactions which lead to the transformation of chromia (Cr_2O_3) into a spinel type mixed oxide (M_3O_4) according to a k_1 rate constant; the second one accounts for all the reactions which lead to the transformation of the M_3O_4 oxide into a Fe_2O_3 oxide according to a k_2 rate constant. If $[M_xO_y]$ is the weight fraction of the oxide phases, it turns out:

$$v_{[Cr_2O_3]} = -\frac{d[Cr_2O_3]}{dt} = k_1[Cr_2O_3] \qquad \text{eq. 8}$$

hence, after integration, the fraction of Cr_2O_3 as a function of time t is given by:

$$[Cr_2O_3]_t = e^{-k_1 t} \qquad \text{eq. 9}$$

Analogously, it turns out:

$$[M_3O_4] = \frac{k_1}{k_2 - k_1}\left(e^{-k_1 t} - e^{-k_2 t}\right) \qquad \text{eq. 10}$$

The quantity of Fe_2O_3 is simply obtained as:

$$[Fe_2O_3] = 1 - [Cr_2O_3] - [M_3O_4] = 1 - e^{-k_1 t} - \frac{k_1}{k_2 - k_1}\left(e^{-k_1 t} - e^{-k_2 t}\right) \qquad \text{eq. 11}$$

The simultaneous fit of the experimental data obtained from Rietveld refinement with the eq. 9, eq. 10 and eq. 11 provided the values of k_1 and k_2, which are respectively $(1.75 \pm 0.2)\ 10^{-4}\ s^{-1}$ and $(4.1 \pm 0.3)\ 10^{-4}\ s^{-1}$. Consequently, it is possible to calculate the relative quantities of the oxides in the oxide layer as a function of time (figure 7).

Several sources of error may influence the value of k_1 and k_2: some experimental (for instance, the possible loss of oxide during the preparation of the samples), and some connected to the simplified model. However, the general trend is in agreement with the models proposed in literature, and it can reasonably describe the experimental observation. In particular, if the fraction of the single oxides are multiplied to the experimental growth curves obtained from TGA measurement obtained at 1050 °C and 0.087 atm of oxygen partial pressure, the weight contributions of the single compounds in the oxide layer can be estimated as a function of time (figure 8). The chromia layer takes about ten minutes to significantly transform into spinel type oxide, and thus to loose its protective behaviour. On the other hand, the spinel type phase reaches the maximum fraction after two hours of treatments, corresponding to the time for typical industrial treatments.

Figure 8 – Measured total weight increase and calculated contribution of the single oxides for a sample treated in industrial-like conditions (0.087 atm of oxygen partial pressure and 1050 °C)

Conclusions

The oxides layer formed on an AISI 304L stainless steel during high temperature oxidation has been described combining experimental and theoretical methods, focusing the attention to the industrial-like conditions. The experimental characterisation confirms the general model described in the literature, with a parabolic growth of the weight and the presence of chromia (Cr_2O_3), hematite (Fe_2O_3) and a mixed spinel type phase (M_3O_4).

According to the mixed parabolic model, the linear and parabolic rate constants were calculated from the TGA curves obtained at different temperature of annealing. From these values, apparent activation energies for the oxidation of the AISI 304L steel were obtained.

From experimental quantitative data and from a simplified model for the oxidation, the relative quantities of the single oxide phases developed in the oxide layer have been estimated as a function of the time.

References

[1] A. M. Huntz, A. Reckmann, C. Haut, C. Severac, M. Herbst, F.C.T. Resende and A.C.S. Sabioni, *Material Science and Engineering A* **447**, 266 (2007)

[2] M. Jepson, PhD thesis (Loughborough University, Loughborough, 2008)

[3] R. Guillamet, J. Lopitaux, B. Hannoyer and M. Lenglet, *Journal of Physics IV* **3**, 349 (1993)

[5] C. E. R. de Carvalho, G. M. da Costa, A. B. Cota and E. H. Rossi, *Material Research Bulletin* **9**, 393 (2006)

[4] N. Karimi, F. Riffard, F. Rabaste, S. Perrier, R. Cueff, C. Issartel and H. Buscail, *Applied Surface Science* **254**, 2292 (2008)

[6] C.Wagner, in *Atom Movements*, (American Society for Metals, Cleveland, 1953), p. 153.

[7] M. Halvarsson, J. Tang, H. Asteman, J. Svensson and L. Johansson, *Corrosion Science* **48**, 2014 (2006)

[8] R. A. Young, *The Rietveld Method* (Oxford University Press, Oxford, 1995)

[9] L. Lutterotti, S. Matthies and H.-R. Wenk, *ICOTOM-12* **1**, 1599 (1999).

[10] R. Luoma, PhD thesis (Acta Polytechnicha Scandinavia, Chem. Tech. Series n. 292, 2002)

[11] A. T. Dinsdale, *Calphad* **15**, 317 (1991)

[12] L. Kjellqvist, M. Selleby and B. Sundman, *Calphad* **32**, 577 (2008)

[13] L. Kjellqvist, Phd thesis (KTH Royal Institute of Technology, Stockholm, 2009)

[14] H. D. Levinstein, M. Robbins and C. Capio, *Material Research Bulletin* **7**, 27 (1972)

[15] U. R. Evans, *The corrosion and oxidation of metals: scientific principles and practical applications* (Edward Arnold, London, 1960)

[16] D. E. Davies, U. R. Evans and J. N. Agar, *Proceedings of the Royal Society A*, 225 (1954) 443

[17] F. J. Pérez, F. Pedraza, M. P. Hierro, J. Balmain, G. Bonnet, *Oxidation of Metals*, 58 (2002) 563

[18] C. Wagner and K. Grunewald, *Zeitschrift fur Physikalische Chemie*, 40 (1938) 455

[19] B.E.Deal, A.S.Grove, *Journal of Applied Physics*, 36 (1965) 3770

[20] M. Jarl and B. Leden, *Proceedings of the International Conference on Process control and Energy Saving in Reheating Furnaces*, 12-14 June, 1985, Lulea, Sweden, 22:1

[21] H. H. Uhlig, *Acta Metallurgica et Materialia* **4**, 541 (1956)

[22] H. M. Hindam and D.P. Whittle, *Oxidation of Metals* **18**, 245 (1982)

[23] S. C. Tsai, A. M. Huntz and C. Dolin, *Material Science and Engineering A* **212**, 6 (1996)

Figure 1
Click here to download high resolution image

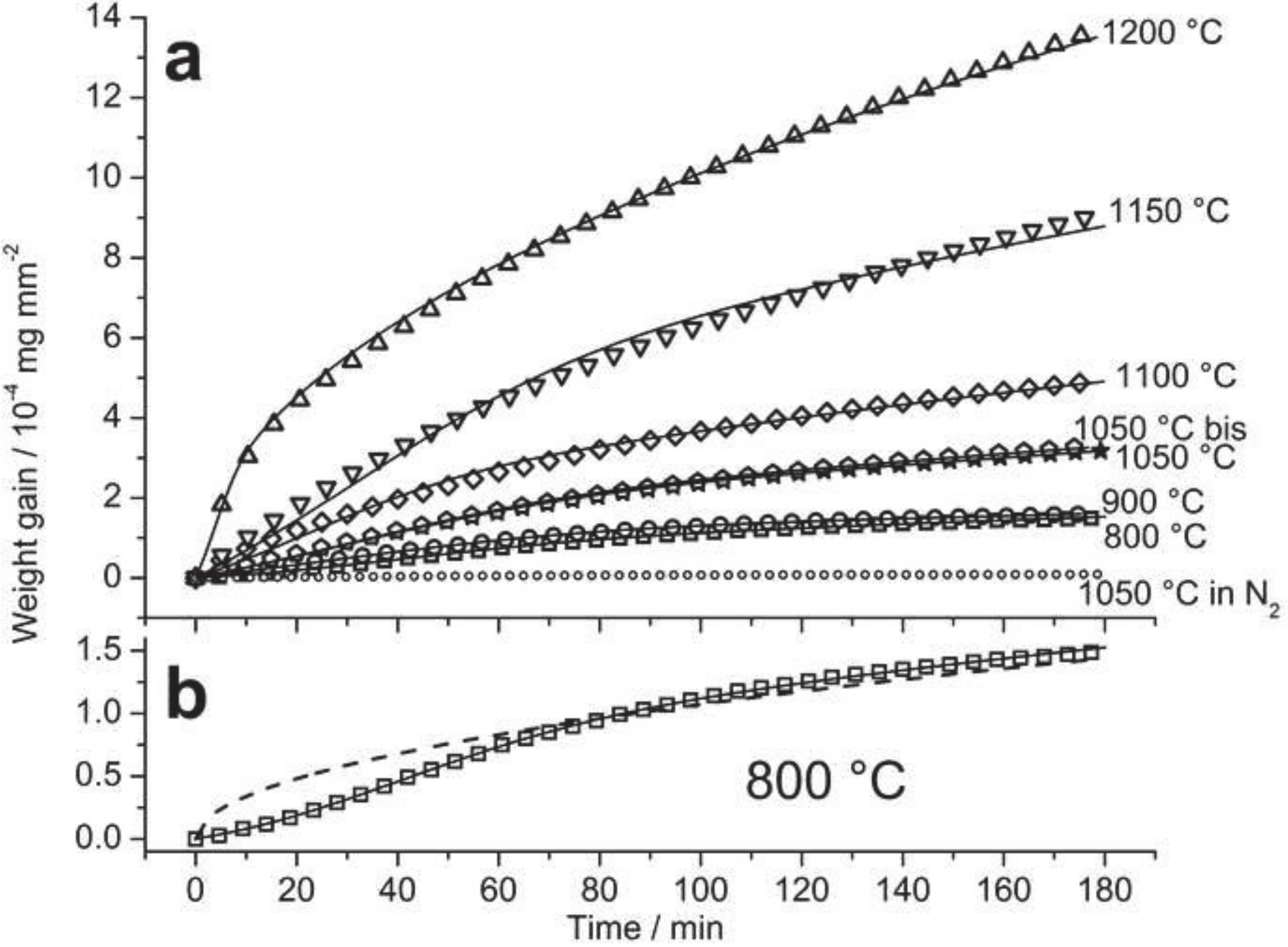

Figure 2
Click here to download high resolution image

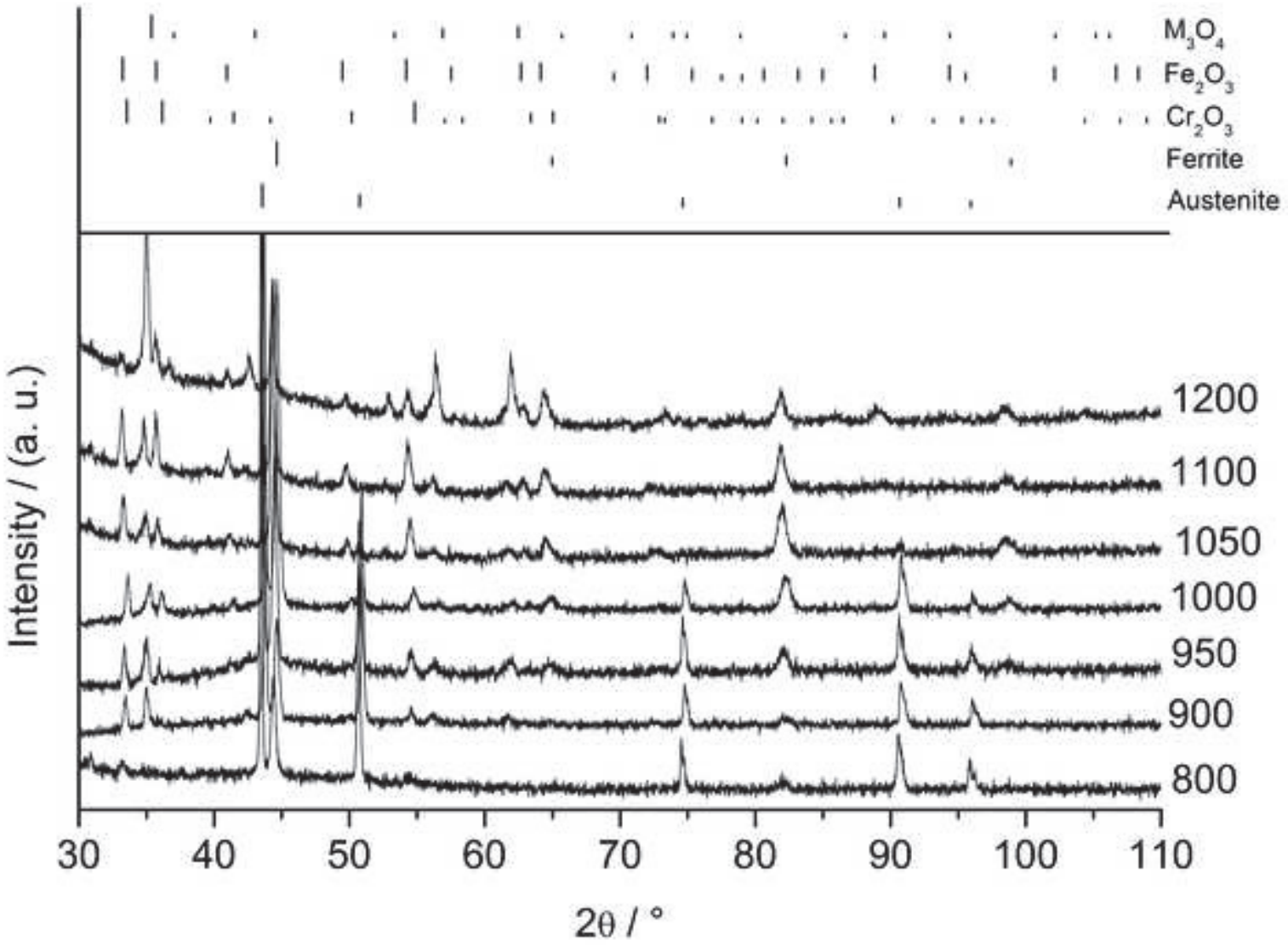

Figure 3
Click here to download high resolution image

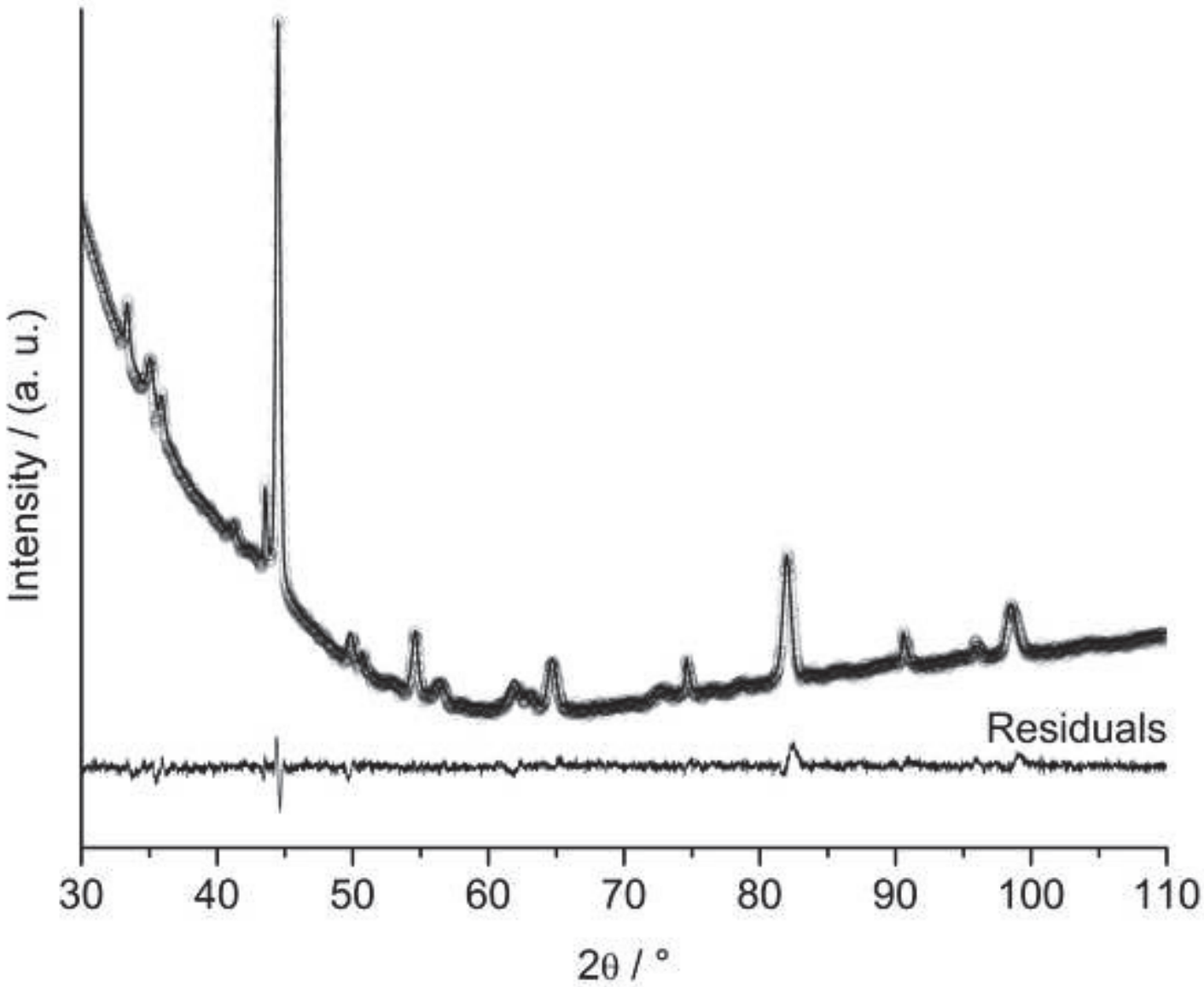

Figure 4a
Click here to download high resolution image

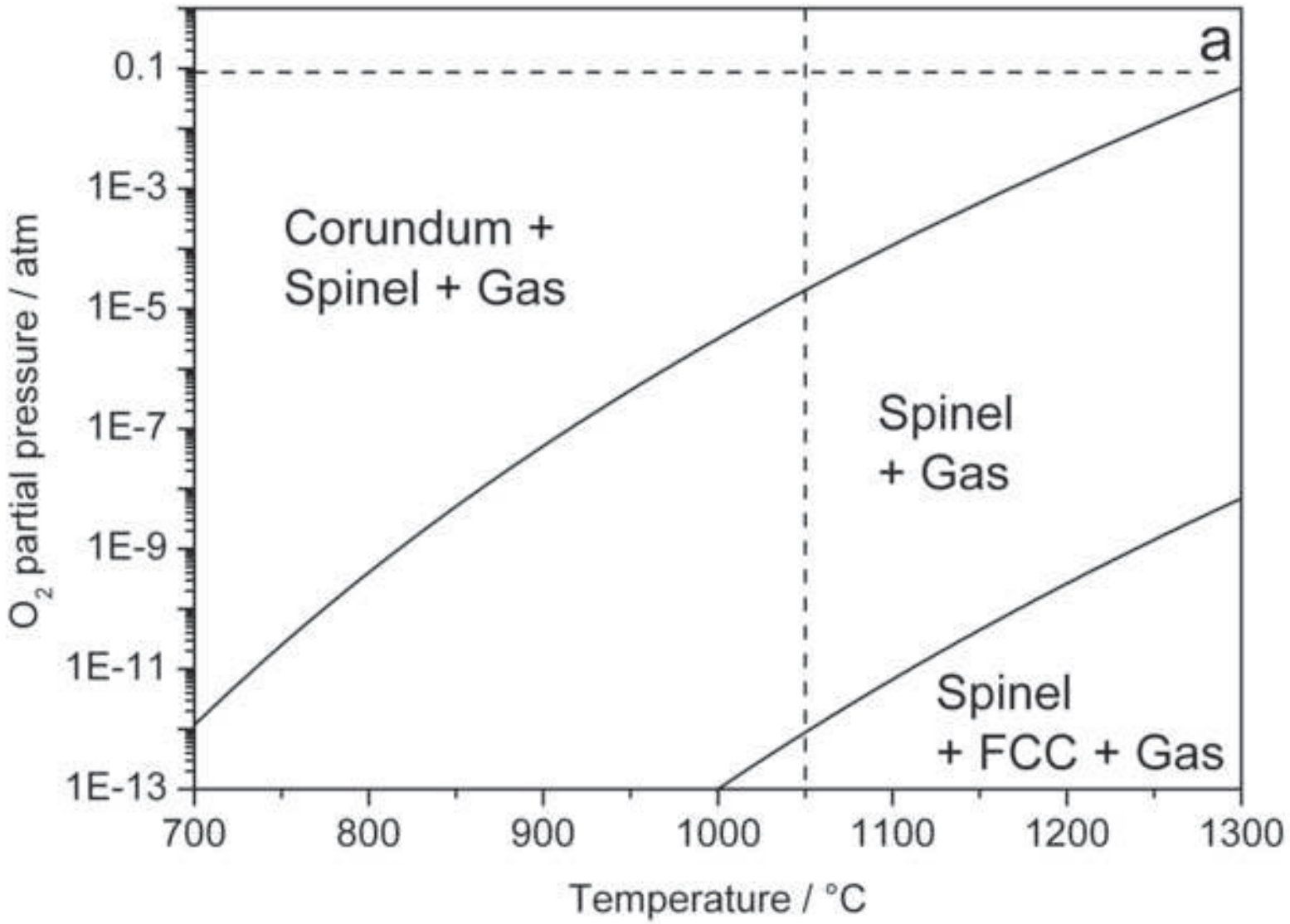

Figure 4b
Click here to download high resolution image

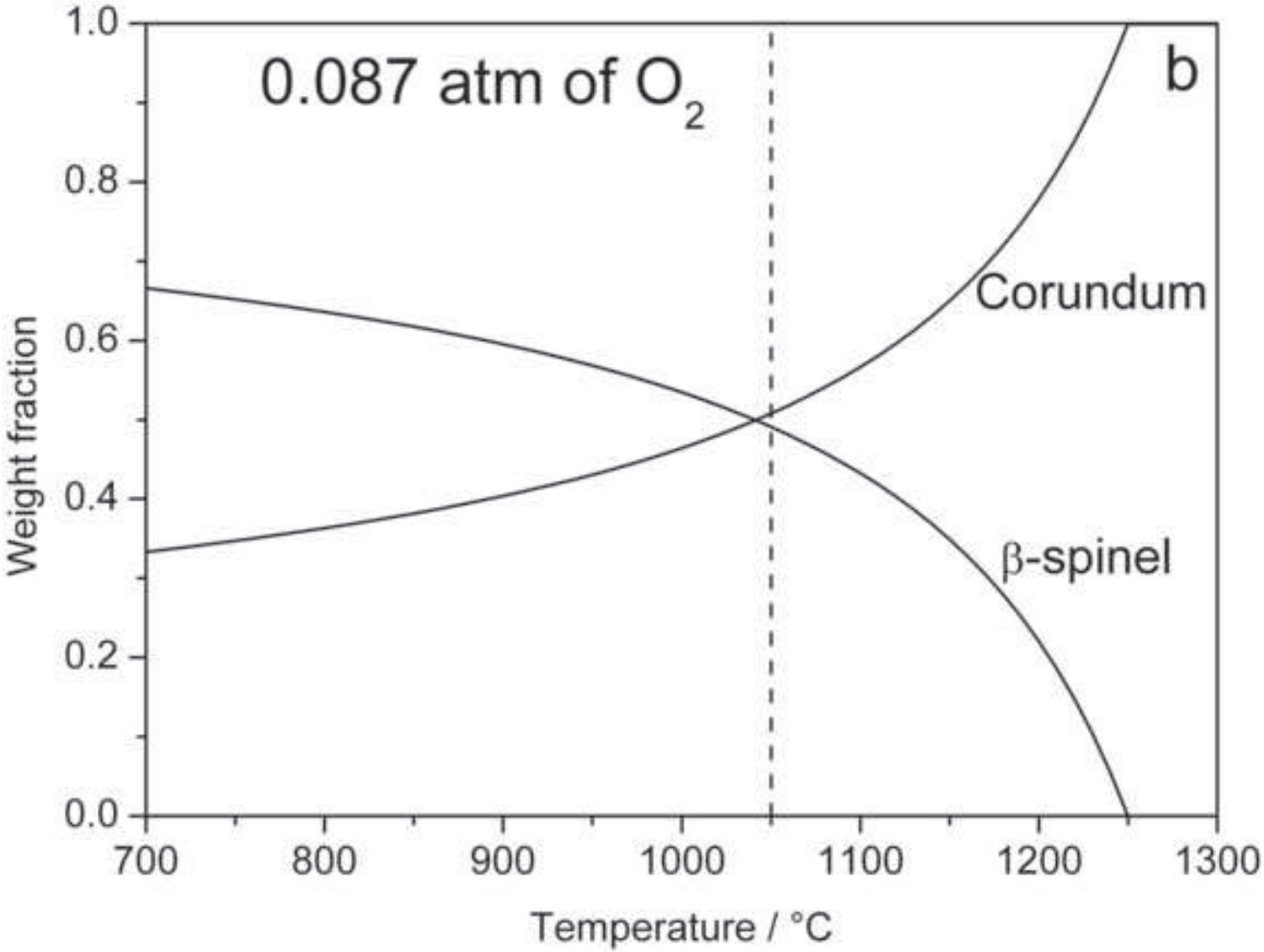

Figure 4c
Click here to download high resolution image

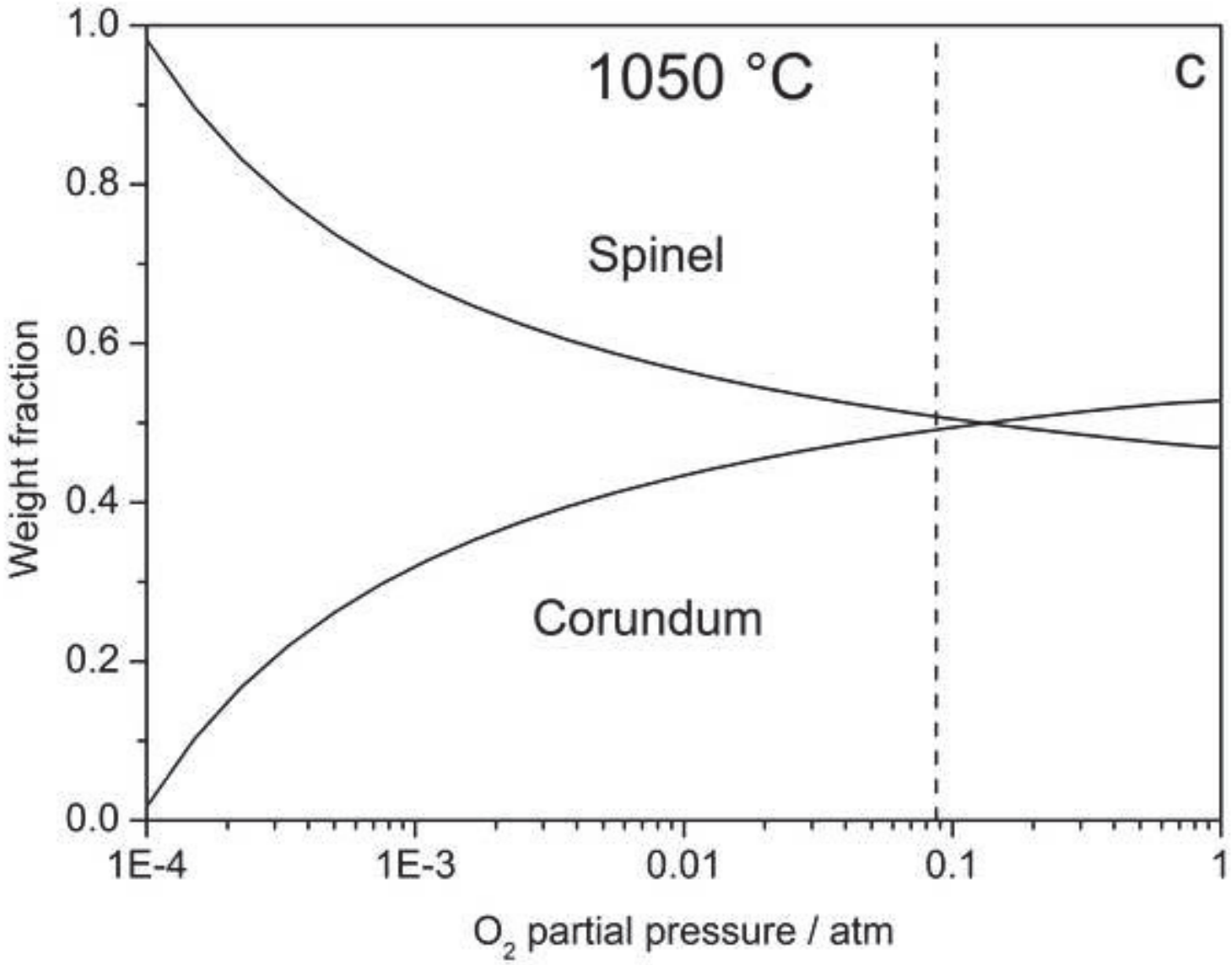

Figure 5
Click here to download high resolution image

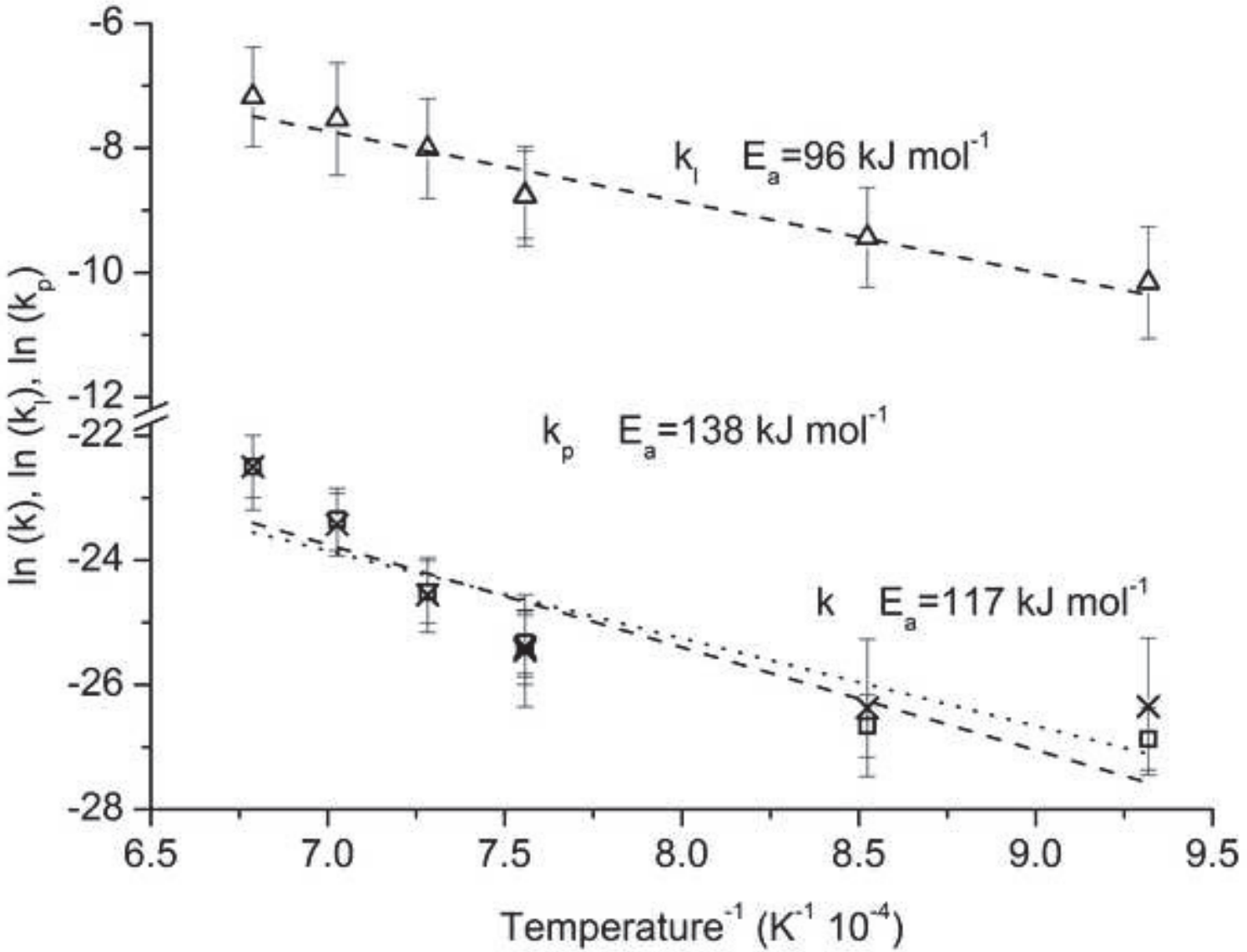

Figure 6
Click here to download high resolution image

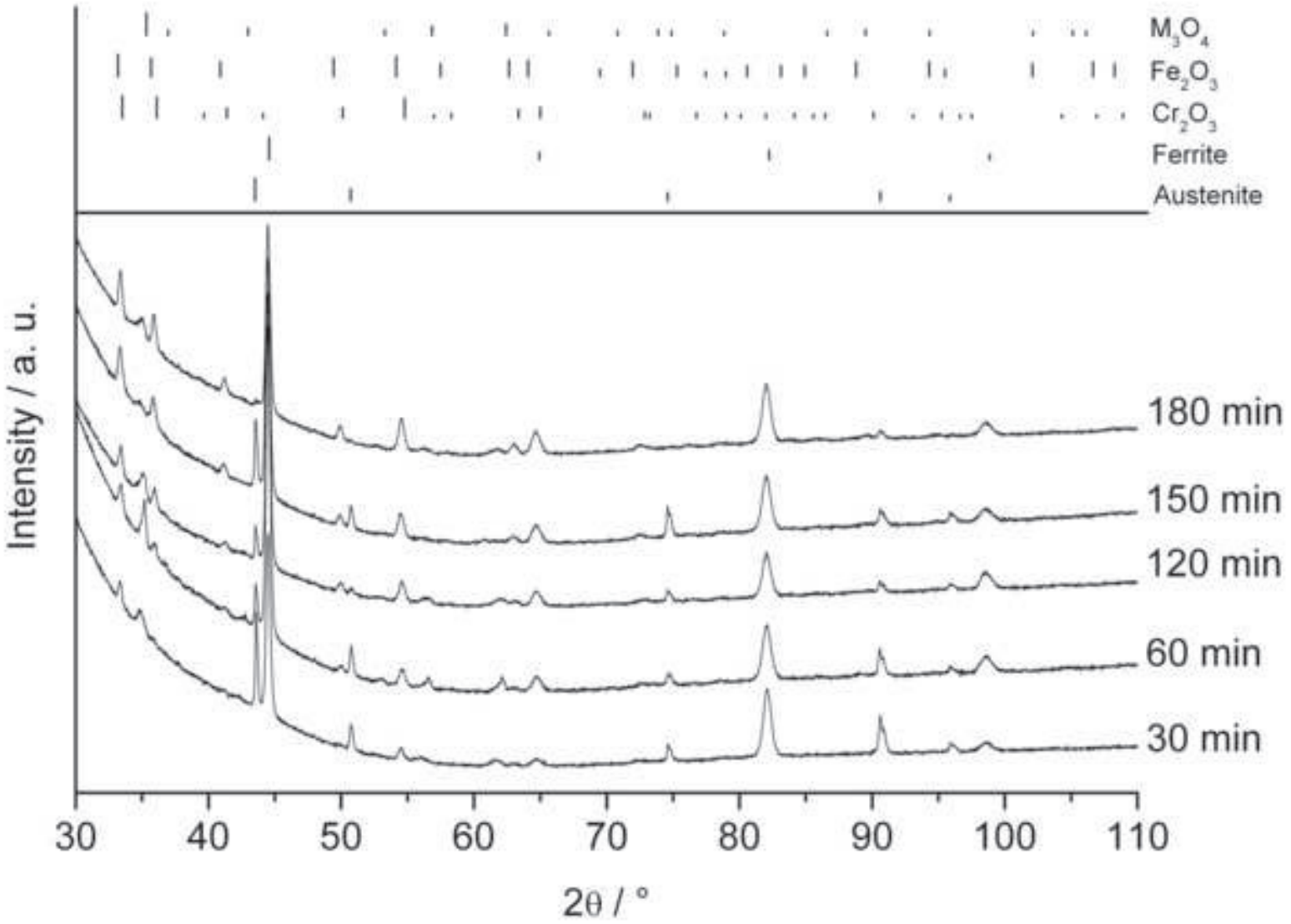

Figure 7
Click here to download high resolution image

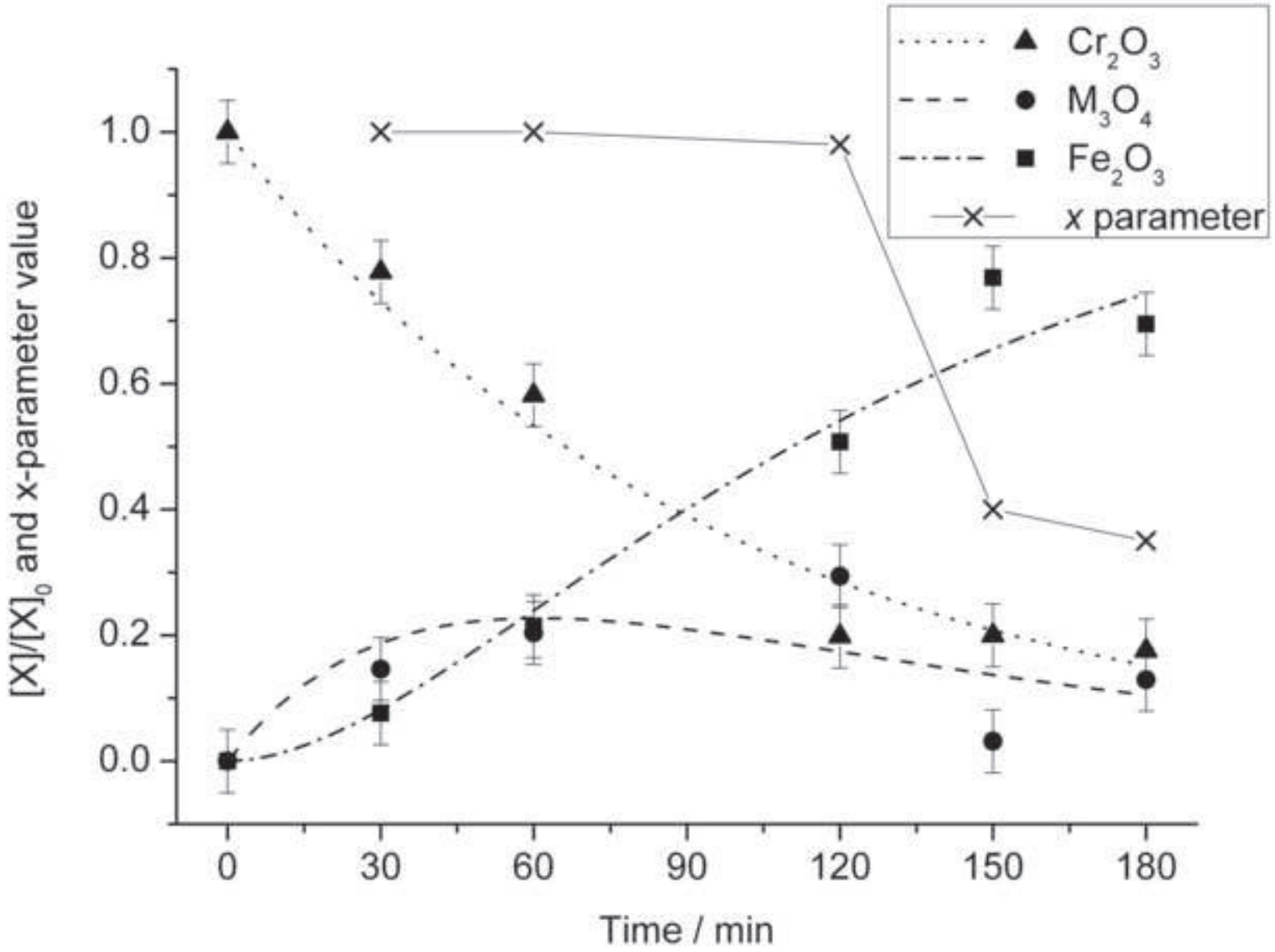

Figure 8
Click here to download high resolution image

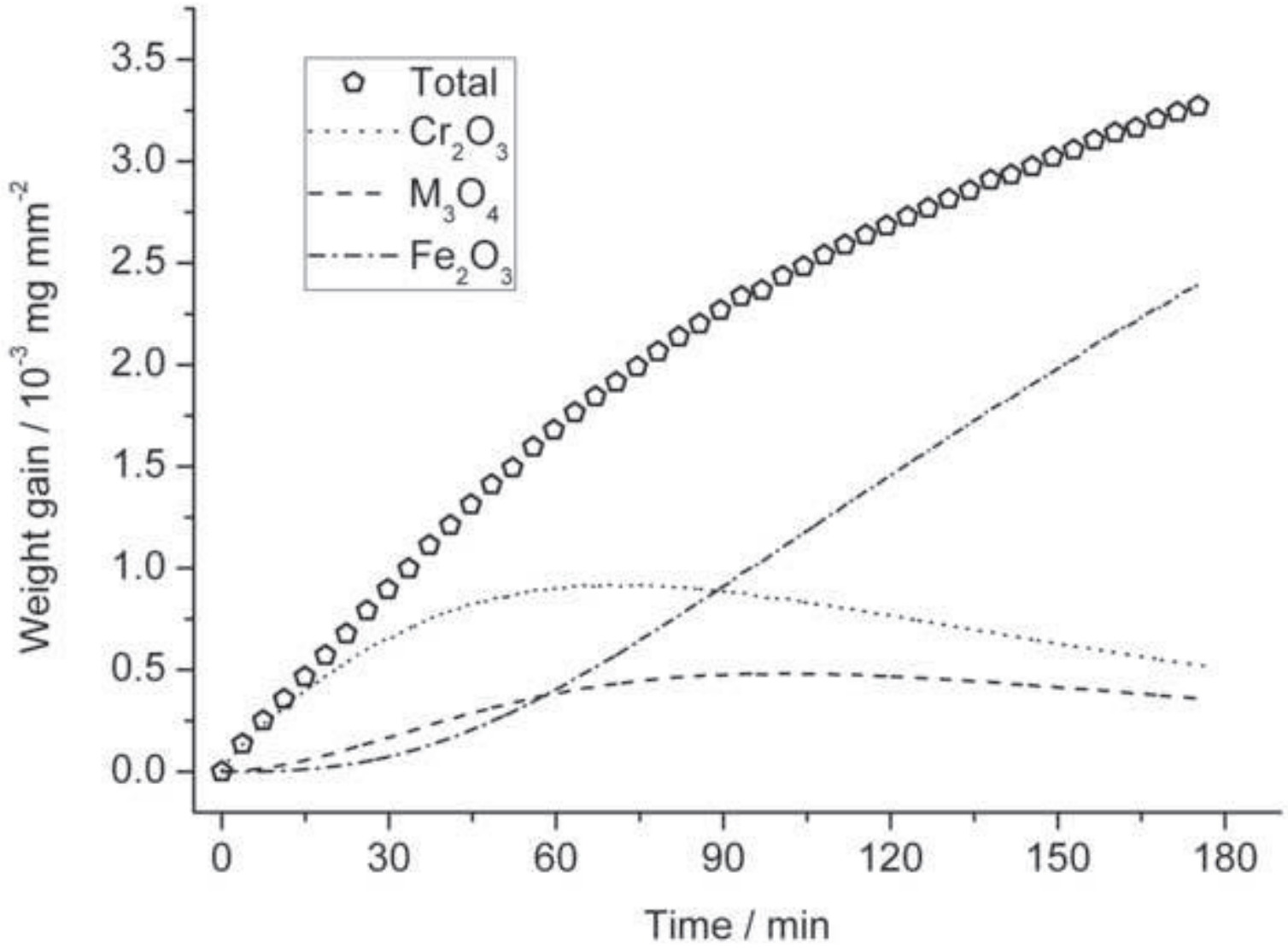

Table 1

C	Cr	Ni	S	Si	Mn	Fe
0.02%	18%	11%	<0.03%	<1%	<2%	Bal.

Table 1 – Composition of AISI 304L stainless steel, wt%

Table 2

Temperature (°C)	800	900	1050	1050 bis	1100	1150	1200
k^2 (g^2 cm^{-4} s^{-1})	$3.6 \cdot 10^{-12}$	$3.5 \cdot 10^{-12}$	$8.8 \cdot 10^{-12}$	$9.3 \cdot 10^{-12}$	$2.3 \cdot 10^{-11}$	$6.7 \cdot 10^{-11}$	$1.7 \cdot 10^{-10}$
σ	6902	5538	3453	3938	2337	1117	55
k_l (mg mm^{-2})	$7.3 \cdot 10^{-6}$	$1.6 \cdot 10^{-5}$	$2.5 \cdot 10^{-5}$	$2.5 \cdot 10^{-5}$	$4.3 \cdot 10^{-5}$	$6.6 \cdot 10^{-5}$	$2.8 \cdot 10^{-4}$
k_p^2 (g^2 cm^{-4} s^{-1})	$2.2 \cdot 10^{-12}$	$2.3 \cdot 10^{-12}$	$9.3 \cdot 10^{-12}$	$1.0 \cdot 10^{-11}$	$2.2 \cdot 10^{-11}$	$7.2 \cdot 10^{-11}$	$1.7 \cdot 10^{-10}$

Table 2 –Rate constant (k) according to eq. 1, and σ parameter, linear constant (k_l) and parabolic constant (k_p) according to eq. 3, obtained from fit of the TGA curves of figure 1

Table 3

Experimental	Cr_2O_3	Fe_2O_3	M_3O_4
$9.75 \cdot 10^{-12}$	$6.95 \cdot 10^{-13}$	$3.81 \cdot 10^{-11}$	$2.69 \cdot 10^{-9}$

Table 3 – Comparison between experimental (k_p^2)and calculated (k_c^2) parabolic rate constants at 1050 °C. The experimental value is the average of the values calculated from the two TGA curves at 1050 °C and 0.087 atm of oxygen partial pressure. Data in $g^2\ cm^{-4}\ s^{-1}$.